Maritime moving target localization using passive GNSS-based multistatic radar

Ma, Hui; Antoniou, Michail; Stove, Andrew; Winkel, Jon; Cherniakov, Mikhail

DOI:
10.1109/TGRS.2018.2838682

License:
Other (please specify with Rights Statement)

Document Version
Peer reviewed version

Citation for published version (Harvard):
Ma, H, Antoniou, M, Stove, AG, Winkel, J & Cherniakov, M 2018, 'Maritime moving target localization using passive GNSS-based multistatic radar', IEEE Transactions on Geoscience and Remote Sensing, vol. 56, no. 8, pp. 4808-4819. https://doi.org/10.1109/TGRS.2018.2838682

Maritime Moving Target Localization Using Passive GNSS-based Multi-static Radar

Hui Ma, Michail Antoniou, Andrew G. Stove, *Senior Member*, *IEEE*, Jon Winkel and Mikhail Cherniakov

***Abstract*—This paper examines the potential in extracting the instantaneous location of maritime moving targets using a passive multi-static radar with Global Navigation Satellite Systems (GNSS) as illuminators of opportunity and a single receiver. The paper presents a theoretical framework for the localization of a moving target from a set of bistatic range measurements. The algorithm and its predicted accuracy are presented. The localization is achieved by what is essentially a multi-lateration technique, which can be applied while the transmitting platform is also in motion. The algorithms and the accuracy predictions, as a function of the number of transmitters, have been experimentally confirmed via a dedicated experimental campaign, where two different maritime targets were detected by up to 12 GNSS satellites belonging to different satellite constellations (GPS, GLONASS and Galileo) simultaneously. To the best of the authors' knowledge, these are the first results of their kind and on this scale not only for GNSS-based passive radar, but for multi-static radar in general.**

***Index Terms*—GNSS-based radar, multi-static radar, target localization.**

I. Introduction

MARITIMEsurveillance is one of the major applications for radar remote sensing systems, active or passive. In recent years, different new approaches for this task have been brought forward, some of which involve active systems based on spaceborne synthetic aperture radar (SAR)[1],airborne radar[2], high-frequency surface-wave radar[3], for example, or passive radars with terrestrial (e.g. DVB-T [4] or GSM [5]) or spaceborne (e.g. Inmarsat [6]) sources.

This paper brings forward a GNSS-based passive radar for this task. This is a new application for GNSS, which adds to their standard use for maritime remote sensing via GNSS reflectometry (GNSS-R), in which the objective is to determine characteristics of the sea such as sea state and wind[7]-[9]. This is also in addition to GNSS-based SAR, which has been used to map fixed objects on land and investigated as a means of monitoring temporal land changes [10]-[13].

As a spaceborne system not originally intended for radar purposes, GNSS-based passive radar lacks the maritime target detection range offered by terrestrial transmitters, such as DVB-T[14] or FM[15], however the global and persistent coverage offered by GNSS offers the capability to provide surveillance in areas where terrestrial illumination sources are not available, such as the open sea, and with an acceptable range resolution (up to15m quasi-monostatic if the GPS L5 or Galileo E5a/b signals are used). In addition, as a passive radar system it is cost-effective since only a receiving segment needs to be built, it does not contribute to electro-magnetic pollution since it re-uses existing GNSS transmissions. However, the main highlight of this technology lies in the number of available satellites. At any time, each GNSS constellation guarantees a minimum of 4 satellites illuminating any point on Earth from different angles, i.e. a minimum of 9 satellites if all 3 GNSS constellations with global coverage, i.e. GPS, GLONASS and Galileo, are considered. More constellations will also enter service in the future. More importantly, all these signals can be acquired by a single receiver and the modest power levels mean they can be separated at the signal processing level, without needing measures to reduce direct path interference, measures which are required in most of other passive radar concepts[16].This is because each GNSS constellation operates on a multiple access scheme (typically Code/Frequency Division Multiple Access, CDMA/FDMA) to discriminate signals from different satellites. This means that GNSS constellations can be inherently considered as multi-static radars with multiple, spatially diverse transmitters and a single receiver, which may introduce a number of advantages for remote sensing. For example, it has already been shown that this spatial diversity can be used to drastically improve spatial resolution in GNSS-based SAR images[17].

At this stage it should also be highlighted that, apart from GNSS being a multi-static radar in its own right, experimental research on multi-static radar in general can be performed using GNSS as it may be relatively easier to develop an experimental test bed with navigation satellites as the transmitting sources, rather than building a multitude of dedicated transmitters and receivers for testing purposes.

In a recent proof of concept study[18], [19], it was experimentally shown that a GNSS-based radar with a single transmitter and a single receiver may identify a moving target in range and in Doppler. The next step in this study is to understand whether or not this radar system can extract the location of a target in motion. Of course this could theoretically be achieved by having a multi-beam receiving system and localizing the target via angle of arrival techniques[20], however that would require a multi-channel receiver that would

compromise the cost-effectiveness of a GNSS-based radar.

Therefore, instead of using spatial diversity on the receiver to provide target location estimates, it is proposed to exploit the spatial diversity on the transmitting side, by considering multiple satellite transmitters under a multi-static radar setup which is one of the main highlights of a GNSS-based system.

In such a multi-static system, the fundamental theory is that it is possible to deduce the instantaneous location of a target if the bistatic ranges between each transmitter, the target and the receiver are known, which can be extracted by the relevant range-Doppler (RD) maps. From the literature it can be found that the analytical solution of the localization problem was firstly derived for source localization based on Time Difference Of Arrival (TDOA)[21]-[23], and then extended to the passive radar case[24]-[27].The target localization problem has been solved for similar multi-static radar systems [24], essentially based on an elliptical positioning, where for each satellite, the target position is constrained to the ellipse defined by foci at satellite and receiver position and the bistatic range from the satellite to the target and, finally, to the receiver. The two main approaches are called the Spherical Interpolation (SI) [28]and Spherical intersection (SX) [29] methods according to their different interpretation. The two methods differ in their implementation, and hence the appropriate accuracy analyses via analytical error equations [30] and Monte Carlo simulations [24] have been performed.

In this paper, target localization is derived based on the SX method for the multi-static GNSS-based radar case, and an analytical accuracy analysis is also outlined. An analytic expression for the expected accuracy of the technique is also produced. This is, of course, very important for the practical utilization of any such technique More importantly, this theoretical work, both the viability of the algorithm and its accuracy, have been confirmed with proof of concept experimental data in a real environment. In this experimental campaign, two different maritime targets were detected by up to 12 GNSS satellites simultaneously, from all 3 major GNSS constellations. In addition, Automatic Identification System (AIS) data were available for both targets as ground truth.

The remaining content of this paper is arranged as follows: Section II discusses the algorithms and accuracy analysis for target localization in GNSS-based radar. Next in Section III, the proof of concept experimental setup and the relevant RD processing results are presented. Section IV presents the experimental target localization results and compares them with ground truth. Finally, a conclusion is given in Section V.

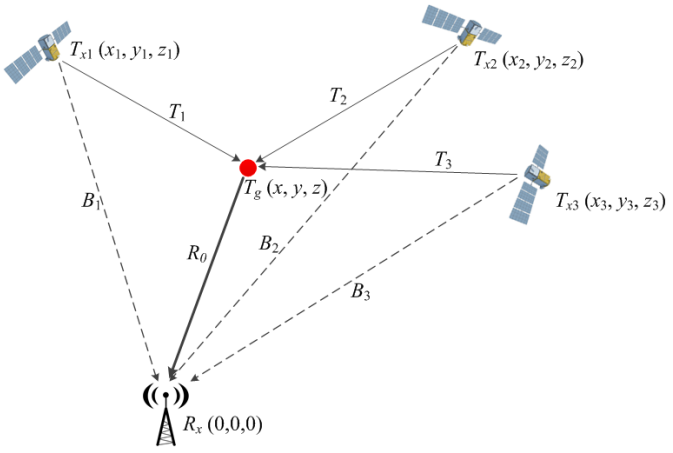

Fig. 1. Multistatic GNSS-based radar (N= 3 in this example).

Notations: We list here some notational convention to be used throughout this paper. Math bold is used for vectors and matrices, to be separated from scalars.

$\boldsymbol{A}^T$	Transpose of $\boldsymbol{A}$
diag(…)	A diagonal matrix with given entries
E($\boldsymbol{A}$)	Expected value of $\boldsymbol{A}$
$\partial \boldsymbol{A}/\partial \boldsymbol{x}$	The partial derivative of $\boldsymbol{A}$with respect to $\boldsymbol{x}$

II. Target Localization with Multi-static Radar

A. Geometry and Problem Description

The system geometry in a local coordinate system is shown in Fig.1. The total number of satellites is represented by$N$. To analyze a multi-static passive radar with multiple transmitters and a single receiver, we can, with no loss of generality, set the origin at the position of the receiver, so the location of the receiver is at the origin$(0,0,0)$. Since the receiver-to-target ranges are relatively short the ground or sea surface is modeled as a flat plane parallel to the (X,Y,0) plane. The coordinates of the target and satellites are denoted as:

$$\boldsymbol{T_g} = \boldsymbol{x} = (\boldsymbol{x}, \boldsymbol{y}, \boldsymbol{z})^{\boldsymbol{T}}, \quad (1)$$

and

$$\boldsymbol{T_{xi}} = \boldsymbol{x_i} = (\boldsymbol{x_i}, \boldsymbol{y_i}, \boldsymbol{z_i})^{\boldsymbol{T}}, \quad (2)$$

with the subscript $i$representing the satellite number.

Hence, the baseline between the i-th satellite and the receiver can be written as:

$$B_i = \|\boldsymbol{x_i}\| = \sqrt{{x_i}^2 + {y_i}^2 + {z_i}^2}, \quad (3)$$

the range between the i-th satellite and the target is:

$$\boldsymbol{T_i} = \|\boldsymbol{x_i} - \boldsymbol{x}\| = \sqrt{(\boldsymbol{x_i} - \boldsymbol{x})^2 + (\boldsymbol{y_i} - \boldsymbol{y})^2 + (\boldsymbol{z_i} - \boldsymbol{z})^2}, \quad (4)$$

and the range between the receiver and the target is:

$$\boldsymbol{R_0} = \|\boldsymbol{x}\| = \sqrt{\boldsymbol{x^2} + \boldsymbol{y^2} + \boldsymbol{z^2}}. \quad (5)$$

When the target is illuminated by multiple satellites simultaneously, the GNSS-based radar can measure the appropriate bistatic target ranges and Doppler, by a basic RD processing. As in the majority of passive/bistatic radar systems, bistatic range is measured based on the difference in time delay between a target echo and the direct signal from the transmitter to the receiver, while bistatic Doppler is measured by the relevant Doppler difference [19].Hence, at the output of the RD processor, for one particular target and particular satellite, the bistatic range may be written as:

$$\boldsymbol{r_i} = \boldsymbol{T_i} + \boldsymbol{R_0} - \boldsymbol{B_i}. \quad (6)$$

The main idea of target localization is to apply multi-lateration techniques based on the difference of bistatic distances in (6).

On condition that all the relative bistatic ranges are measured accurately, we can lock the target onto its correct position. This can be solved by matrix method as following.

By rearranging (6), we have:

$$r_i + B_i - \sqrt{x^2 + y^2 + z^2} = \sqrt{(x_i - x)^2 + (y_i - y)^2 + (z_i - z)^2}. \quad (7)$$

After squaring the equation and a rearrangement, we obtain:

$$\frac{1}{2}\left[\boldsymbol{B_i^2} - (\boldsymbol{r_i} + \boldsymbol{B_i})^2\right] + (\boldsymbol{r_i} + \boldsymbol{B_i}) \cdot \boldsymbol{R_0} = \boldsymbol{x^T x_i}, \quad (8)$$

which can be expressed as:

$$\boldsymbol{Ax} = \boldsymbol{K} + \boldsymbol{C}\|\boldsymbol{x}\|, \quad (9)$$

where A is the transmitter position matrix:

$$\boldsymbol{A} = \begin{bmatrix} \boldsymbol{x_1} \\ \boldsymbol{x_2} \\ \vdots \\ \boldsymbol{x_N} \end{bmatrix}_{\boldsymbol{N\times 3}}. \quad (10)$$

Kisconstant vector denoted as:

$$\boldsymbol{K} = \frac{1}{2}\begin{bmatrix} \boldsymbol{B_1^2} - (\boldsymbol{r_1} + \boldsymbol{B_1})^2 \\ \boldsymbol{B_2^2} - (\boldsymbol{r_2} + \boldsymbol{B_2})^2 \\ \vdots \\ \boldsymbol{B_N^2} - (\boldsymbol{r_N} + \boldsymbol{B_N})^2 \end{bmatrix}_{\boldsymbol{N\times 1}}, \quad (11)$$

and C is the sum of two constant vectors R and$B$, respectively denoting the radar measured bistatic ranges and baselines:

$$\boldsymbol{C} = \boldsymbol{R} + \boldsymbol{B} = \begin{bmatrix} \boldsymbol{r_1} \\ \boldsymbol{r_2} \\ \vdots \\ \boldsymbol{r_N} \end{bmatrix}_{\boldsymbol{N\times 1}} + \begin{bmatrix} \boldsymbol{B_1} \\ \boldsymbol{B_2} \\ \vdots \\ \boldsymbol{B_N} \end{bmatrix}_{\boldsymbol{N\times 1}}. \quad (12)$$

As the only one unknown quantity in (9), the target position vector x can be given by the solution of (9).

It is well known that the most basic solutions to this problem, with only a small number of baselines can lead to 'ghost' solutions as well as the real one, but when the number of satellites, i.e., in general, the number of bistatic range measurements, becomes greater than the dimensionality of the space (in our case, three dimensions) the ghost solutions vanish.

B. General Solution Derivation

The left side of (9) conforms to the standard form of a linear equation set, however the right side contains a function of the unknown parameter, in the form of its determination as $\|\boldsymbol{x}\|$. For solving this equation set, we use the Spherical-Intersection (SX) method. Firstly, we ignore the existence of $\|\boldsymbol{x}\|$ in the right side of (9) and regard it as constant. Therefore, we can get a preliminary solution of $\boldsymbol{x}$ as:

$$\boldsymbol{x} = (\boldsymbol{A^T A})^{-1}\boldsymbol{A^T}(\boldsymbol{K} + \boldsymbol{C}\|\boldsymbol{x}\|). \quad (13)$$

We introduce two variables:

$$\boldsymbol{a} = (\boldsymbol{A^T A})^{-1}\boldsymbol{A^T K}, \quad (14)$$

$$\boldsymbol{b} = (\boldsymbol{A^T A})^{-1}\boldsymbol{A^T C}, \quad (15)$$

where a and b are vectors with size of 3×1. Then we have:

$$\boldsymbol{x} = \boldsymbol{a} + \boldsymbol{b}\|\boldsymbol{x}\|. \quad (16)$$

Substituting (16) into the equation of $\|\boldsymbol{x}\|^2 = \boldsymbol{x^T x}$, and after rearranging, we get the following quadratic equation for$\|\boldsymbol{x}\|$:

$$(\boldsymbol{b^T b - 1})\|\boldsymbol{x}\|^2 + \boldsymbol{2a^T b}\|\boldsymbol{x}\| + \boldsymbol{a^T a} = \boldsymbol{0}. \quad (17)$$

Hence, we can solve the receiver-to-target range as:

$$\boldsymbol{R_0} = \|\boldsymbol{x}\| = \frac{-\boldsymbol{a^T b} \mp \sqrt{(\boldsymbol{a^T b})^2 - (\boldsymbol{b^T b - 1})\boldsymbol{a^T a}}}{(\boldsymbol{b^T b - 1})}. \quad (18)$$

Then x can be obtained by substituting $\|\boldsymbol{x}\|$ into (30).

C. Accuracy Analysis

To estimate the accuracy of the value obtained for the target location, we regard the error resulting from the measured error of bistatic ranges. The accuracy of the bistatic ranges depends on the range resolution, range cell and Signal-to-Noise Ratio (SNR). Based on this, we can use σ_{ri}^2 to represent the variance of the bistatic range from the i-th satellite. Then the covariance matrix is:

$$\boldsymbol{\Sigma_{N\times N}} = \boldsymbol{E}[\boldsymbol{RR^T}] - \boldsymbol{E}[\boldsymbol{R}](\boldsymbol{E}[\boldsymbol{R}])^T = \mathbf{diag}\left(\left[\boldsymbol{\sigma_{r1}^2}, \boldsymbol{\sigma_{r2}^2}, \dots, \boldsymbol{\sigma_{rN}^2}\right]\right). \quad (19)$$

The target location varies only with the bistatic ranges; however, no explicit expression is available for the covariance calculation, because of the term $\|x\|$ in (9). We therefore refer to the method in [10, 22] to derive an approximate expression. Using a first-order Taylor series expansion, the covariance matrix of the target location becomes:

$$\boldsymbol{X_{3\times 3}} = \boldsymbol{E}[\boldsymbol{xx^T}] - \boldsymbol{E}[\boldsymbol{x}](\boldsymbol{E}[\boldsymbol{x}])^T = (\boldsymbol{\partial x/\partial R})\boldsymbol{\Sigma}(\boldsymbol{\partial x/\partial R})^T, \quad (20)$$

with $(\boldsymbol{\partial x/\partial R})_{N\times 3}$ being the Jacobian matrix. The Jacobian can be derived from the (9) as:

$$\boldsymbol{A}(\boldsymbol{\partial x/\partial R}) = \boldsymbol{\partial K/\partial R} + \boldsymbol{\partial}[(\boldsymbol{R} + \boldsymbol{B})\|\boldsymbol{x}\|]/\boldsymbol{\partial R}. \quad (21)$$

From (11), we can get:

$$\boldsymbol{\partial K/\partial R} = -\mathbf{diag}([\boldsymbol{r_1} + \boldsymbol{B_1}, \dots, \boldsymbol{r_N} + \boldsymbol{B_N}]) = -\boldsymbol{\Gamma}. \quad (22)$$

And the second term of the right-hand of (21) is:

$$\boldsymbol{\partial}[(\boldsymbol{R} + \boldsymbol{B})\|\boldsymbol{x}\|]/\boldsymbol{\partial R} = \boldsymbol{I}\|\boldsymbol{x}\| + (\boldsymbol{R} + \boldsymbol{B})(\boldsymbol{x^T}/\|\boldsymbol{x}\|)\,\boldsymbol{\partial x/\partial R}. \quad (23)$$

By substituting (22-23) into (21) and re-arranging, we can express the Jacobian matrix as:

$$\boldsymbol{\partial x/\partial R} = (\boldsymbol{\Delta^T \Delta})^{-1}\boldsymbol{\Delta^T}[\boldsymbol{I}\|\boldsymbol{x}\| - \boldsymbol{\Gamma}], \quad (24)$$

with

$$\boldsymbol{\Delta} = \boldsymbol{A} - \ (\boldsymbol{R} + \boldsymbol{B})(\boldsymbol{x^T}/\|\boldsymbol{x}\|), \quad (25)$$

which gives an explicit expression for the covariance when substituted into (34).

It should be noted here that the variance of the target location is calculated considering only the first order of the Taylor expansion, that is, the linear component.

III. Experimental Setup and Range-Doppler Maps

A. Experimental Setup, Scene and Parameters

An experimental campaign was carried out to confirm the proposed technique and assess its performance. A passive receiver tuned to acquire GNSS signals was installed to the east of Portsmouth harbor in the UK. This was the SX3 receiver [31], manufactured by IFEN GmbH, a software-defined radio receiver designed for GNSS navigation, which we specifically customized for operation as a passive radar receiver. The bandwidth of the receiver covered the following GNSS bands: GPS L1, GLONASS G1, and Galileo E5a and E5b. All four bands were recorded at a sampling rate of 20 MHz. Fig.3 shows a photograph of the experimental setup taken during the measurement.

The receiver was equipped with two channels, named as the reference and radar channels. The reference channel was connected to a low gain antenna to receive the direct signals from all satellites in its field of view. On the other hand, the radar channel used antennas pointed towards the target area. Since the Galileo E5 bands are separated in frequency with

regards to GPS-L1/GLONASS-G1, two separate high-gain (15 dB) antennas connected via a splitter were used to receive these bands.

As a proof-of-concept experiment, the receiver was based on the shore rather than in open sea and large targets moving relatively close to the receiver were sought to provide a sufficiently high SNR. At the time of measurement, two such targets of opportunity were present. Both of them were commercial ferries of different (but large in both cases) sizes and following different trajectories, which are running on a regular schedule so their departure and arrival times to the harbor were known in advance. The speed of both targets was low as they entered port. In addition, both targets were equipped with AIS, which could be used as a reference for comparing multi-static localization results. Those were recorded in real-time via an available AIS receiver. Figure 4 shows the tracks of the ferries and the relative position of the receiver, super-imposed on a Google Earth photograph. The first ferry ("Target A") was the "St. Cecilia", with dimensions 77m in length and 17.2m in beam (Fig. 5 (a)), and the second ferry ("Target B") was the "Bretagne", with dimensions 158mx26m (Fig. 5 (b)).

Throughout the recording periods each ferry was continuously illuminated by twelve (Target A) and eleven satellites (Target B), respectively. Information on these satellites can be found in Table I. The set includes two Galileo satellites, four Glonass satellites and six GPS satellites. The reflected signal of Sat 9 (GPS – BIIR05) is seen only for 'St Cecilia' but except for that, both 'Bretagne' and 'St Cecilia' are detected by the receiver using all remaining 11 satellites.

B. Range-Doppler Processing Results

Following data acquisition, a set of bistatic RD maps for each target were generated from each transmitter in Table I. The RD processor used has been discussed in detail in [19] so only its brief description will be provided here to avoid duplication.

As a first stage, a signal synchronization process is applied, whereby the receiver tracks all the parameters of the direct signal (delay, Doppler, phase navigation message and secondary code, if available) from each satellite in the field of view of the antenna at the reference channel. Following that, a local replica of the direct signal which was then used as the reference signal for matched filtering with radar channel data over the duration of a single GNSS ranging code. The duration of this code is 1ms and this is thus the effective Pulse Repetition Interval (PRI). Following this operation, a Fourier Transform over the Coherent Processing Interval (CPI), or observation time, was performed to obtain the target's RD map as well as maximize SNR. A few comments should also be made on the parameters of the signal processing algorithm summarized above. The processing scheme requires that the highest Doppler frequency of interest has a period much greater than the correlation time. For example at a speed of 10 ms^{-1} (20 kn) and a typical GNSS carrier frequency of 1.5 GHz the maximum Doppler shift is 100 Hz, i.e. a period of 10 ms, so the 1ms correlation period ensures that the detection of moving ships will not be compromised. After range compression, the SNR has been improved by the time-bandwidth product of the signal (typically 40 dB), but further integration of multiples of the 1 ms period is still both necessary to extract target Doppler and maximize SNR, which is achieved by the Fourier Transform over the CPI. Noting that since the satellites yield different bistatic ranges and Doppler frequencies, the RD processing needs to be applied to each individual satellite independently.

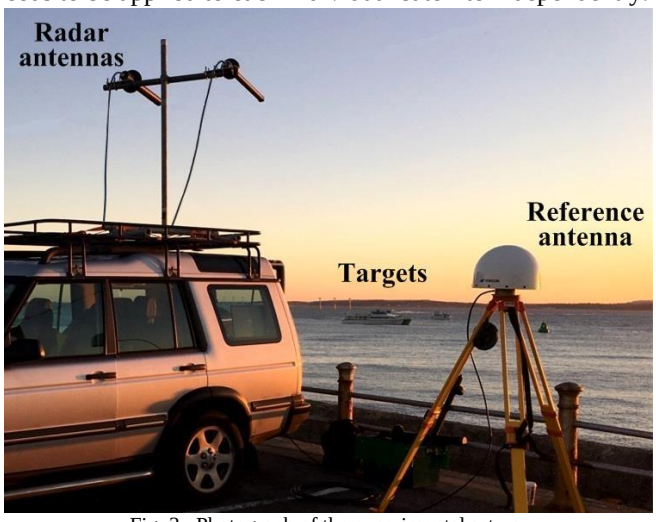

Fig. 3. Photograph of the experimental set up.

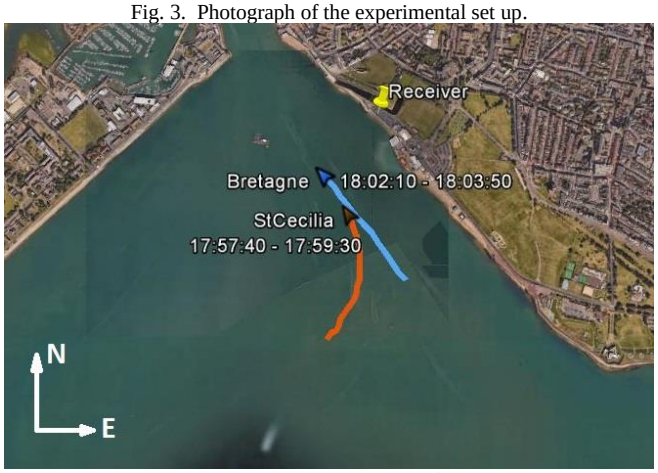

Fig. 4. Ferry tracks during the experiment (from GoogleEarth).

(a)

(b)

Fig. 5. Photograph of the ferries: Target A – St Cecilia and Target B - Bretagne

TABLE I EXPERIMENTAL AND SIGNAL PROCESSING PARAMETERS

Parameter		Value	
		Target A	Target B
Sat 1	Constellation and number	Galileo – GSAT0206 (PRN30)	
	Bistatic angle	69.9° ~ 63.8°	79.1° ~ 56.5°
	Azimuth(relative to North)	63.8° ~ 63.1°	62.0° ~ 61.4°
	Elevation(relative to radar)	55.2° ~ 54.7°	54.0° ~ 53.5°
Sat 2	Constellation and number	Galileo – GSAT0211 (PRN02)	
	Bistatic angle	30.1° ~18.6 °	50.0° ~ 5.5°
	Azimuth(relative to North)	40.27° ~ 40.33°	40.45° ~ 40.53°
	Elevation(relative to radar)	7.3° ~ 6.7°	5.9° ~ 5.4°
Sat 3	Constellation and number	Glonass – COSMOS2457	
	Carrier frequency	1599.75 MHz	
	Bistatic angle	78.0° ~ 82.7 °	74.6° ~ 89.3°
	Azimuth(relative to North)	314.2° ~ 313.6°	312.4° ~ 311.6°
	Elevation(relative to radar)	67.8° ~ 68.8°	70.2° ~ 71.1°
Sat 4	Constellation and number	Glonass – COSMOS2425	
	Carrier frequency	1602.00 MHz	
	Bistatic angle	59.5° ~54.9 °	66.7° ~ 50.2°
	Azimuth(relative to North)	42.4° ~ 42.1°	41.6° ~ 41.4°
	Elevation(relative to radar)	53.5° ~ 52.5°	51.1° ~ 50.2°
Sat 5	Constellation and number	Glonass – COSMOS2477	
	Carrier frequency	1604.8125 MHz	
	Bistatic angle	54.7° ~ 66.0°	36.6° ~ 81.4°
	Azimuth(relative to North)	317.9° ~ 318.1°	318.4° ~ 318.6°
	Elevation(relative to radar)	16.1° ~ 16.9°	18.2° ~ 18.9°
Sat 6	Constellation and number	Glonass – COSMOS2459	
	Carrier frequency	1600.3125 MHz	
	Bistatic angle	65.7° ~78.3 °	47.1° ~ 96.4°
	Azimuth(relative to North)	305.4° ~ 304.7°	303.7° ~ 303.1°
	Elevation(relative to radar)	5.1° ~ 4.5°	3.7° ~ 3.2°
Sat 7	Constellation and number	GPS – BIIR02 (PRN13)	
	Bistatic angle	85.2° ~ 89.6°	78.2° ~ 94.7°
	Azimuth(relative to North)	293.2° ~ 293.9°	295.1° ~ 295.8°
	Elevation(relative to radar)	66.8° ~ 67.6°	68.8° ~ 69.6°
Sat 8	Constellation and number	GPS – BIIR04 (PRN20)	
	Bistatic angle	84.5° ~ 93.4°	72.9° ~ 105.9°
	Azimuth(relative to North)	289.0° ~ 288.0°	286.4° ~ 285.5°
	Elevation(relative to radar)	46.4° ~ 46.8°	47.4° ~ 47.8°
Sat 9	Constellation and number	GPS – BIIR05 (PRN28)	
	Bistatic angle	102.1° ~ 92.9°	113.6° ~ 79.8°
	Azimuth(relative to North)	118.0° ~ 117.1°	115.6° ~ 114.7°
	Elevation(relative to radar)	44.2° ~ 44.8°	45.6° ~ 46.0°
Sat 10	Constellation and number	GPS – BIIF05 (PRN30)	
	Bistatic angle	68.4° ~ 61.9°	79.0° ~53.8 °
	Azimuth(relative to North)	63.7° ~ 63.5°	63.2° ~ 63.1°
	Elevation(relative to radar)	52.6° ~ 51.8°	50.6° ~ 49.9°
Sat 11	Constellation and number	GPS – BIIRM04 (PRN15)	
	Bistatic angle	84.2° ~ 93.7°	68.1° ~ 106.0°
	Azimuth(relative to North)	288.1° ~ 288.3°	288.7° ~ 289.0°
	Elevation(relative to radar)	35.4° ~ 36.2°	37.3° ~ 38.0°
Sat 12	Constellation and number	GPS – BIIRM06 (PRN07)	
	Bistatic angle	50.2° ~ 39.5°	69.0° ~ 25.6°
	Azimuth(relative to North)	58.1° ~ 58.3°	58.6° ~ 58.8°
	Elevation(relative to radar)	19.6° ~ 18.9°	17.9° ~ 17.2°
GPS L1 band carrier frequency		1575.00 MHz	
Galileo E5 carrier frequency		1176.45 MHz (E5a) 1207.24 MHz (E5b)	
GPS C/A code bandwidth		1.023 MHz	
Glonass P code bandwidth		5.11 MHz	
Galileo E5 single channel bandwidth		10.23 MHz	
Sampling frequency		20 MHz	
Pulse repetition interval		1millisecond	
Coherent processing interval		2.5 second	
Non-coherent processing interval		10 second	

The CPI of course also determines the Doppler resolution. As the CPI increases from 1 ms, the SNR improves linearly because of a strong coherence between adjacent slow-time samples of the same range bin. There are however three limits to the extent to which the integration time can be increased.

The most extreme limit is the time for which the target remains visible.

The next limit is the rate at which the radar is required to deliver information to whoever or whatever is to make use of this information.

The third limitation is the kinematics of the target – its motion will cause the signal to move from one range cell to the next, and its acceleration will cause it to move from one Doppler bin to another – an effect which also gets more significant because the Doppler bins become narrower as the integration time increases.

To achieve longer integration times than the ones reported here, additional range alignment and phase compensation for changes in the Doppler shift are needed during signal processing [18]. An appropriate CPI was selected as 2.5 s, through a simple practice of progressively increasing it and recording the resulting SNR, until the point where the SNR gain starts to deviate from the coherent integration (linear) case.

The limit in the integration time is probably caused by the range walk. For a range cell length of 15m, which is compatible with the 10 MHz bandwidth of the signals, then if it takes 2.5s for the target to move through half a range cell its speed must be 3ms^{-1}, of 6 kn, which is probably about right for a ship near a port.

If we look further at the kinematic limit to the integration time, we can consider the time for an accelerating target to move through one Doppler bin, given that the Bistatic Doppler frequency shift is [32]:

$$f_d{}^b = \frac{2v\cos(\beta/2)\cos\theta}{\lambda}, \tag{26}$$

and assuming that the change of bistatic geometry is negligible within the integration time. Then for a target which accelerates at a rate a, the change in bistatic Doppler shift in time T will be:

$$\Delta f_d = \frac{2aT\cos(\beta/2)\cos\theta}{\lambda} \xrightarrow{\beta,\theta\to 0} \frac{2aT}{\lambda}. \tag{27}$$

The limiting value occurs when this change of Doppler equals the monostatic Dopler resolution, $1/T_{\text{int}}$, giving a maximum correlation time of

$$T_{\text{int}}^{\max} = \sqrt{\frac{\lambda}{2a}}. \tag{28}$$

Since the wavelengths are of the order of 23 cm, we can deduce that the maximum acceleration of the targets was of the order of 0.02 ms^{-2} (1 kn every 25 seconds) so they were moving at close to a constant speed. In fact it is possible that the limiting factor

was spread of the target Doppler due to vibration caused by the engines.

As a final step, 4 sets of adjacent RD maps, each obtained with a CPI of 2.5 s, are non-coherently combined , for a further suppression of fluctuations in the background noise level, resulting in the total data acquisition time of 10 s.

The RD maps for targets A and B are shown in Fig.6 and Fig.7, composed of results obtained from 12 or 11 satellites

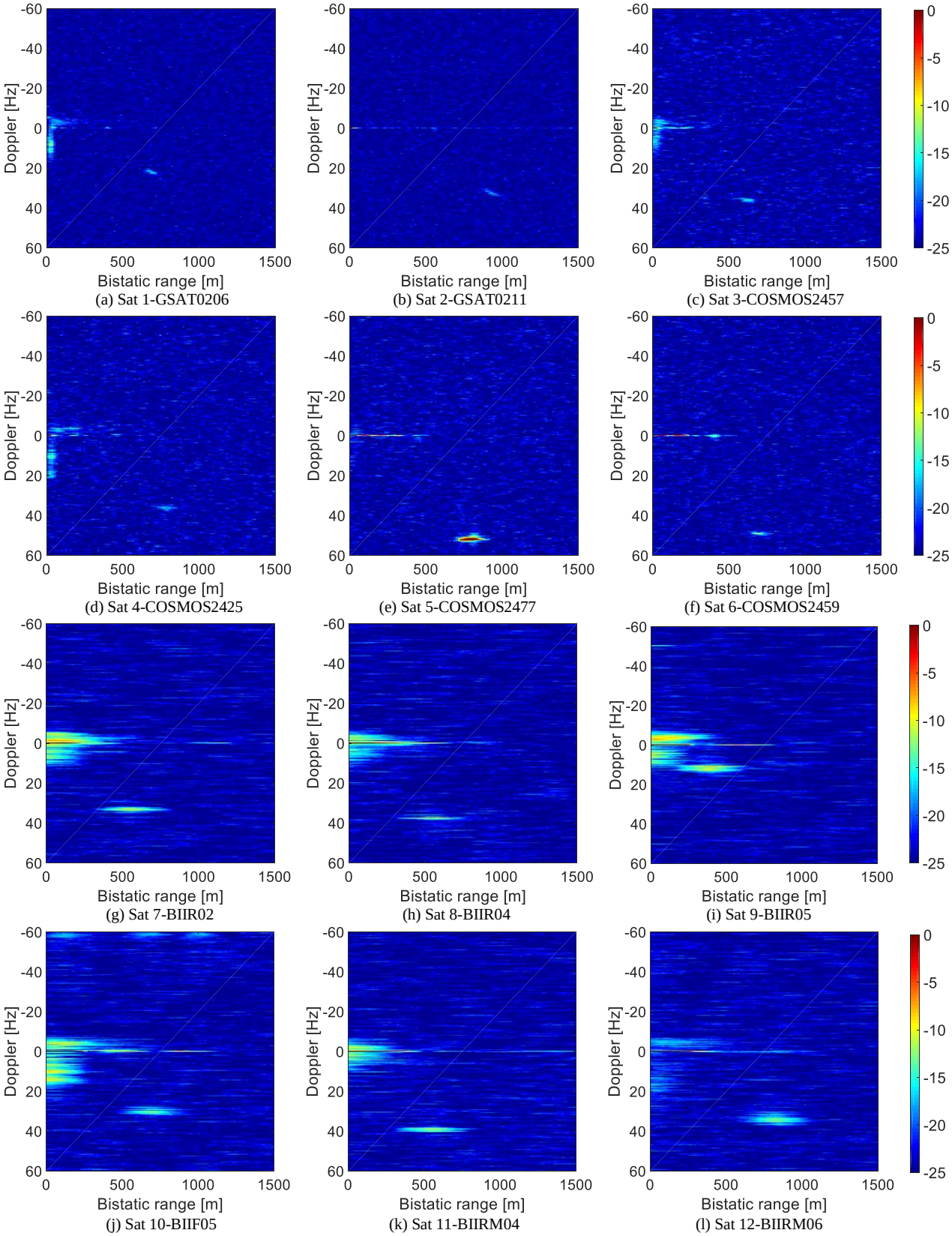

Fig. 6. RD maps of Target A by different satellites at the same time. Each RD map is non-coherent summation of 4 sets of adjacent RD maps with CPI of 2.5 s.

respectively. For example, Fig. 6 shows the simultaneous detections of Target A, obtained with individual Galileo, GLONASS and GPS satellites. In all cases, the colourscale is in decibels, with 0 dB representing the highest intensity in each RD map, and a dynamic range artificially clipped to -25 dB. In all cases, 0 dB appears at zero range and zero Doppler, which is the direct satellite signal received through the radar antenna sidelobes, as expected. Sidelobes of the direct signal are visible

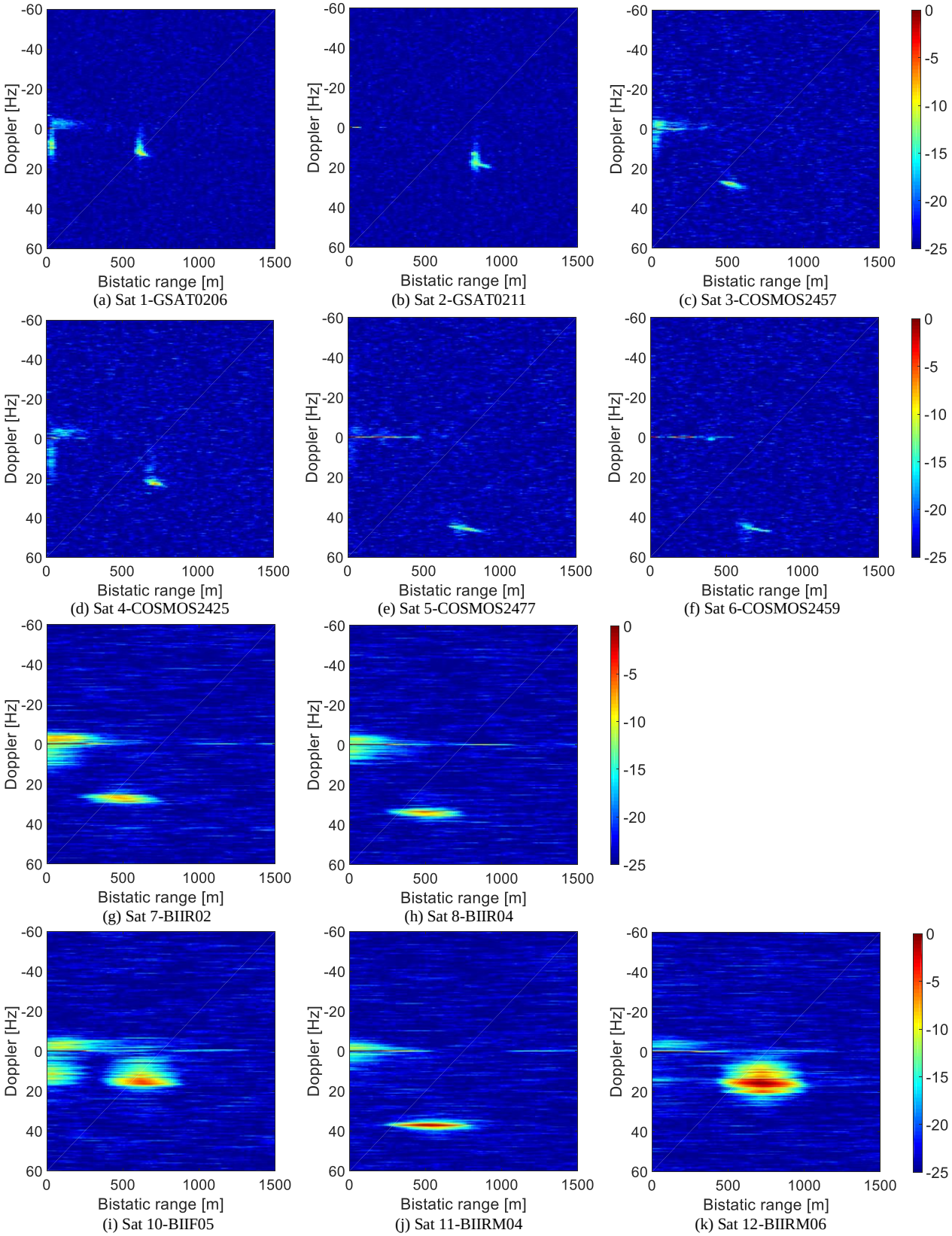

Fig. 7. RD maps of Target B by different satellites at the same time. Each RD map is non-coherent summation of 4 sets of adjacent RD maps with CPI of 2.5 s.

throughout the zero Doppler line. Returns at close ranges but spread in Doppler are attributed to sea clutter.

Comparing the RD maps, it can first of all be seen that the same target appears to be at a different bistatic range and Doppler for different satellites, as expected due to the difference in bistatic geometry and the difference in carrier frequencies across the GPS, GLONASS and Galileo bands used. It should be stated here that in an operational case where multiple targets are simultaneously detected, it may be a formidable task to associate multiple bistatic detections to a particular target in question. However, this is a subject for further study which is beyond the scope of this paper. Looking at RD maps of the same target, it also interesting to mention (albeit in passing) that even for the same constellation type (e.g. GLONASS in Fig. 6 (d)-(f)), the relative intensity of the target and the clutter can vary considerably, which may introduce benefits for target detection in the future.

One of the most pronounced differences across RD maps obtained by different satellite constellations is the available range resolution, since the signal bandwidths used are substantially different (Table 1). These also cause return signal intensities to vary. For example, the GPS L1 signal with a 1 MHz bandwidth gives a 150 m range resolution, which is larger than the largest dimension of target A and comparable to that of target B, whereas for Galileo E5a with a 10 MHz bandwidth a range resolution cell corresponds to just a portion of a target.

IV. Experimental Multi-static Target Localization

A. *Bistatic Ranges Extraction*

Since target responses were well separated to those of clutter, the implementation of Moving Target Indication algorithms (e.g. [33]) was beyond the scope of this work. Having a single pronounced target return, one can then trace its bistatic range (and Doppler) history of each target relative to each satellite, by extracting the peak of the target response in each RD map at consecutive CPIs. Figures 8 and 9 show the extracted bistatic ranges of targets A ("St Cecilia") and B ("Bretagne"), respectively. Sets of markers in the same type give the bistatic ranges versus time for each satellite. The bistatic range calculated from the AIS ground truth is shown by the continuous curve. For brevity, bistatic ranges for six satellites are plotted in each figure, separated vertically so the relative errors between range histories from different satellites can be seen (at the expense of not showing the absolute range values on the graph itself but providing some information on the graph

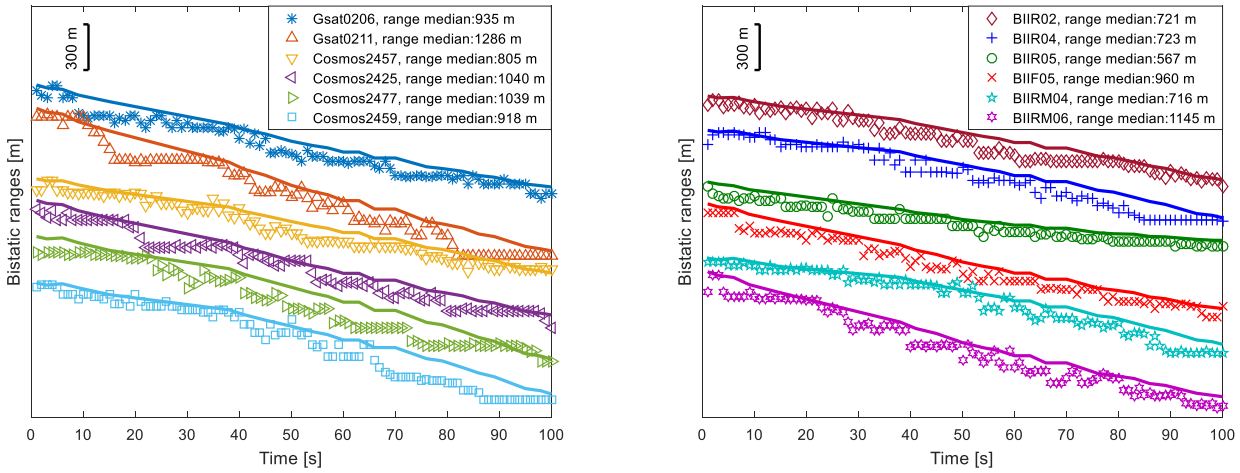

Fig. 8. Bistatic ranges detected for Target A (the ferry 'St Cecilia') with different satellites.

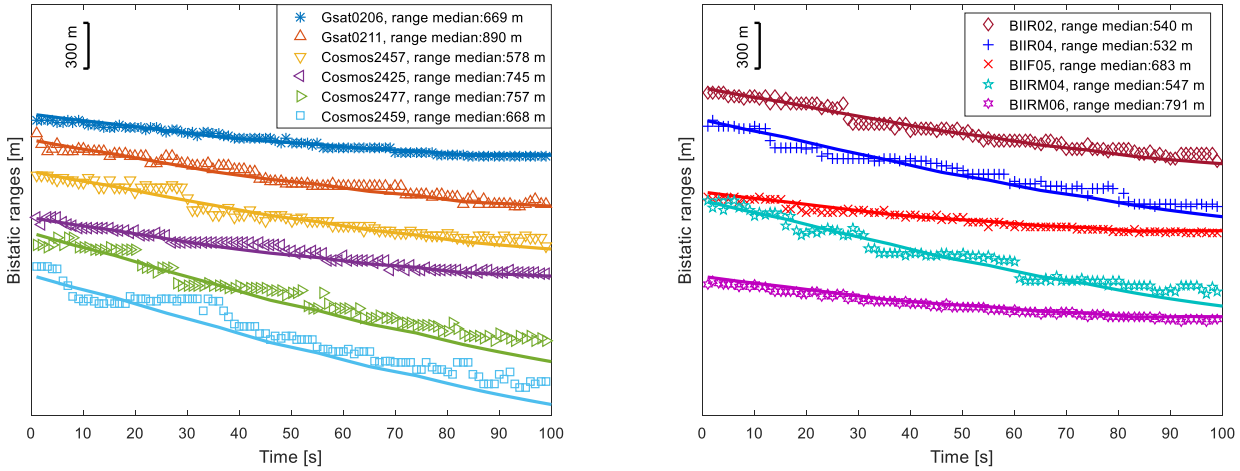

Fig. 9. Bistatic ranges detected for Target B (the ferry 'Bretagne') with different satellites.

legends).Using the location of the peak value to estimate range means that the data are bound by the range sampling accuracy, which translates to 15m for a sampling frequency of 20 MHz. Note that in principle this could be avoided by estimating the 'centre of gravity' of the detection but the complexity of this refinement was not considered worthwhile for this proof of concept test. The satellite information and the median bistatic range for each curve is given in the figure's legend. Taking Sat1 (GSAT0206) as an example, in the left figure of Fig.9, the blue curve occupies a range of 750 m along the vertical axis, as can be seen from the scale bar. The median range is given as 935 m, so we can see that the bistatic range for Sat1 gradually decreases from around 1310 m to 560 m during the dwell time of 110 s.

When comparing the experimentally measured bistatic ranges and their AIS references, we can observe firstly the high degree of the coincidence in the curves. The difference between experimental bistatic range and theoretical values is within the range of 100 m, which is within the range of the expected deviation. Note that the location of the AIS system onboard these extended targets does not necessarily coincide with the area on the ship providing the strongest reflection across all satellites, so there may be bias between theoretically predicted and experimental results. Results are further degraded by the AIS accuracy, which for positional information is usually that of GPS, so while a comparison between expected and experimental results should be made there are real factors affecting it.

There are also some obvious deviation between the measured bistatic range and the AIS reference for some tracks at some times, e.g, between 10 s to 40 s for Sat2 (GSAT0211) and Sat4 (COSMOS2425). In these sections, the bistatic ranges remain almost unchanged while AIS reference changes steadily. This is believed to be due to changes in the geometry between the ship's AIS position reference point and the position of the strongest reflection from the target. This is a consequence of the target's maneuvering. Likewise, Fig.10 shows similar results for the estimated bistatic ranges for Target B (the ferry Bretagne). Although the Target B is much larger than Target A, a higher degree of agreement between detected range and AIS reference can be seen compared to the results of Target A. This is because, as we can see from fig.4, that whilst Target A was maneuvering, Target B was sailing in a straight line.

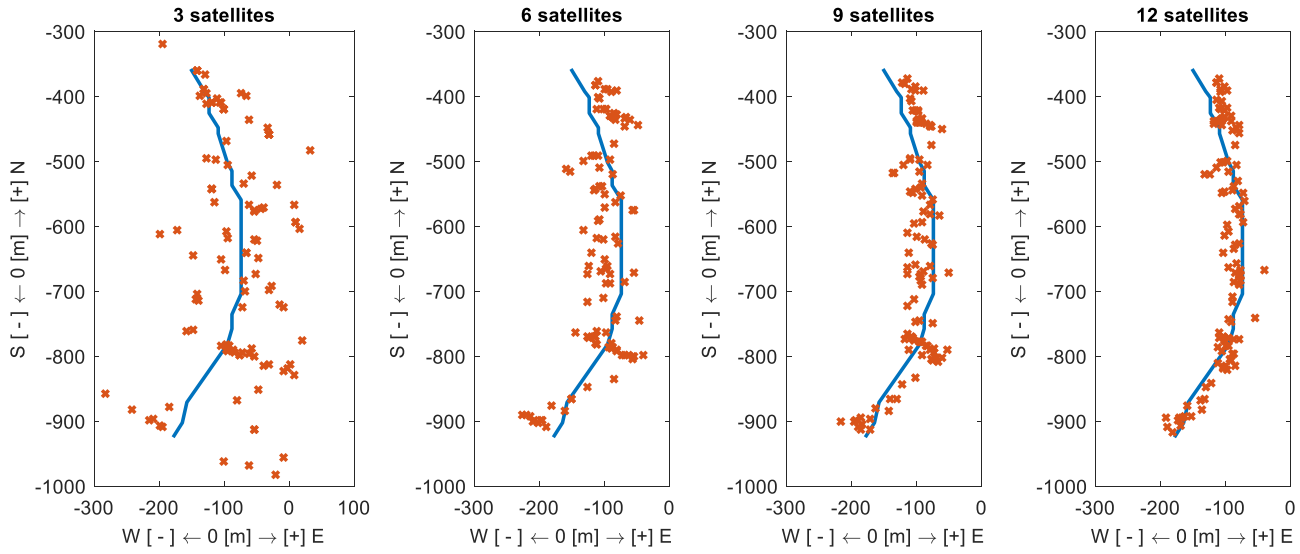

Fig. 11. Bistatic ranges detected for Target A with different satellites.

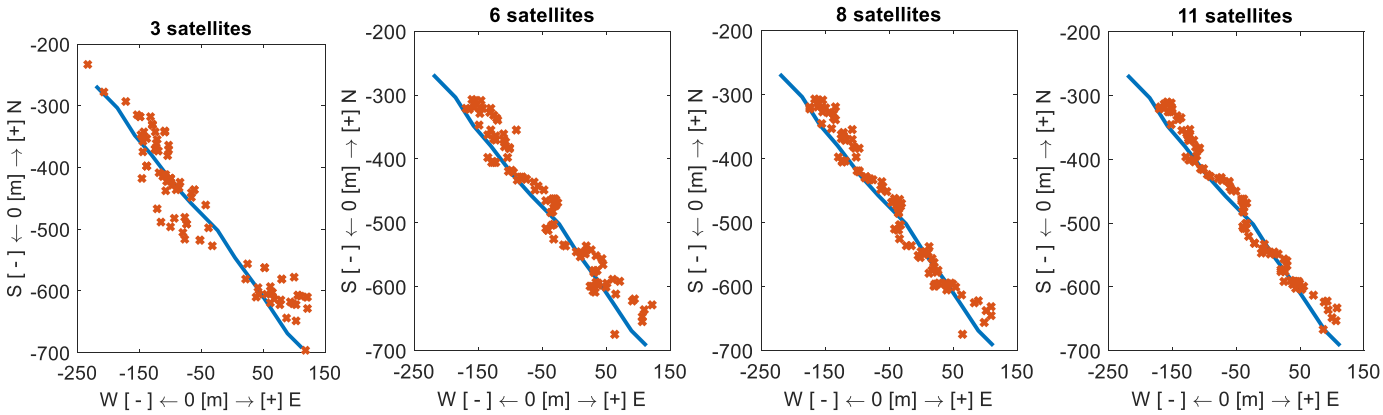

Fig. 12. Bistatic ranges detected for Target B with different satellites.

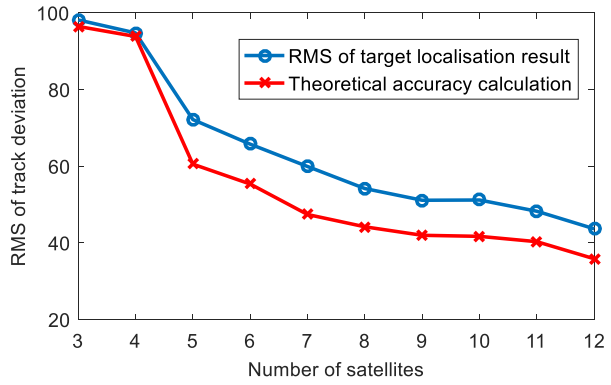

Fig. 13. RMS of target localisation result for Target A.

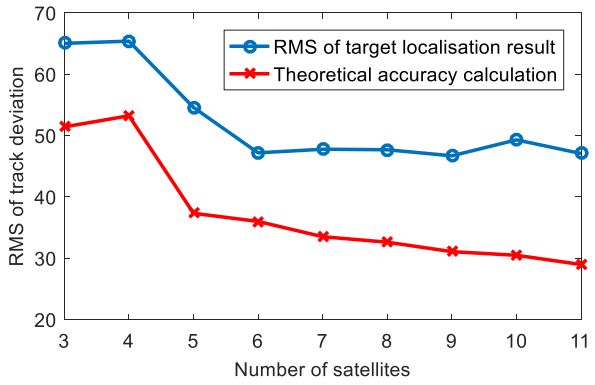

Fig. 14. RMS of target localisation result for Target B.

B. Target Localization Results

Based on the measured bistatic ranges seen from multiple satellites, we can localize the target at any particular time. By applying the method in Section II, we obtained the target localization results for the two targets with increasing numbers of satellites up to the maximum of 12 or 11, in the two cases. The results are illustrated in Fig.11 and Fig.12 for Target A and B respectively. These figures are 'North Up,' so East is to the right, i.e. the same orientation as in Fig.4. In these figures, the red '×' marks show all the obtained target location with a step of 1 s using a certain number of satellites. The blue continuous lines are the AIS track serving as the ground truth. For both Target A and Target B, a series of results contains four figures, with each figure titled with the increasing number of satellites used. The number of satellites is counted from Sat1 and following the order listed in Table I.

Comparing the two figures it can be seen that the proposed approach can correctly localise targets in both cases. It also shows that as the number of satellites increases, the target is localised more accurately, as expected, even if the target is manoeuvring (Fig.11). To get a numerical understand of the improvement of target localization performance as the number of satellites increases, we calculated the Root Mean Square (RMS) of the detected track deviations in cases of different numbers of satellites, using AIS track as the reference. Of course since the AIS tracks are not identical to the actual tracks extracted by the RD maps (as well as other issues explained above), the theoretical accuracy results should serve as the upper performance limit. Figures 13 and 14 give the RMS calculation results for the two targets respectively, in comparison with the corresponding theoretically calculated reference using the method mentioned in Section II.C.

From Fig.13-14, we can observe a good degree of coincidence between the measured RMS and the theoretical results. This confirms the accuracy estimation method for the target localization. Since the detected bistatic ranges deviate from the AIS reference, the theoretical versus expected results may not be identical (see for example Fig. 13), but the trend is very similar. It is also shown that even though the same satellites are used to localize both targets and the SNR is sufficiently high, the relative accuracy improvement is not the same. This indicates that in practice the performance improvement also depends on target characteristics (for example orientation or kinematics) apart from those of the transmitter. The method of multi-lateration has therefore been verified by experimental results as being usable for target localization in multi-static radar. This is valid for GNSS-based passive radar in specific, but also for multi-static radar in general, active or passive.

V. Conclusions

This paper has been the first to show that passive multi-static radar based on GNSS transmissions can be used to determine the instantaneous position of a target. This can be achieved by exploiting the spatial diversity provided by GNSS constellations while using a single receiver. Algebraic equations on the basis of the mature spherical intersection method have been derived in order to do so. Theoretical results have been supported by a dedicated, proof of concept experimental campaign with maritime targets. In this campaign, two different targets with different trajectories were detected by up to 12 different GNSS satellite transmitters simultaneously, which to the authors' knowledge is the first experimental measurement of this kind at such a scale.

Experimental results confirm the functionality of the concept as well as the expected performance, which can be extended from passive multi-static GNSS-based radar to any multi-static radar, active or passive.

It is very important to demonstrate that it is possible to go from the bistatic range-Doppler plots obtainable from a single transmitter to actually locate the target. We have shown this, but there are surprisingly few other descriptions of passive radars which show that this step can actually be achieved. At the same time, it brings GNSS-based radar experimental test beds forward as a means of testing general multi-static radar theory, due to the relative ease of experimentation with GNSS as opposed to building a dedicated multi-static system with a large number of transmitters and receivers

We have also proved that we can meet the predicted accuracy for such a location process, which is also of great importance for the practical utilization of passive radars. The

results show that as the number of transmitters increases, localization performance may also increase, but the upper limit of transmitters needed varies with target kinematics.

Now that the capability in localizing objects with this system has been confirmed, the next stage in research is to investigate how multi-static radar systems can be used to indicate the kinematic state of a target.

ACKNOWLEDGEMENT

Work on the conversion of the SX3 to a passive radar receiver was supported under a contract of the European Space Agency in the frame of the Announcement of Opportunities on GNSS Science and Innovative Technology within the European GNSS Evolutions Programme (EGEP ID 89).

REFERENCES

[1] M. Stasolla, J. J. Mallorqui, G. Margarit, C. Santamaria, N. Walker,"A comparative study of operational vessel detectors for maritime surveillance using satellite-borne synthetic aperture radar,"*IEEE J. Sel. Topics Appl. Earth Observ. in Remote Sens.*, vol. 9, no.6,pp. 2687-2701, Jun. 2016.

[2] A. Damini, M. McDonald, G. E. Haslam,"X-band wideband experimental airborne radar for SAR, GMTI and maritime surveillance,"*IEE Proceedings-Radar, Sonar and Navigation*, vol. 150, no.4, pp. 305-312,Aug. 2003.

[3] S. Maresca, P. Braca, J. Horstmann, R. Grasso,"Maritime surveillance using multiple high-frequency surface-wave radars," *IEEE Geosci. Remote Sens. Lett.*, vol. 52, no.8, pp. 5056-5071,Aug. 2014.

[4] D. Langellotti, F. Colone, P. Lombardo, E. Tilli, M. Sedehi, A. Farina,"Over the horizon maritime surveillance capability of DVB-T based passive radar," in*IEEE Microwave Conference (EuMC), 2014 44th European*,Rome, Italy, Oct. 2014.

[5] R. Zemmari, M. Daun, M. Feldmann, U. Nickel,"Maritime surveillance with GSM passive radar: Detection and tracking of small agile targets,"In *International Radar Symposium (IRS)*, Dresden, Germany, Jun. 2013.

[6] M Golabi, A Sheikhi, M Biguesh, "A new approach for sea target detection in satellite based passive radar," in*Iranian Conference on Electrical Engineering (ICEE)*, Mashhad, Iran, 2013, pp. 1-5.

[7] J. F. Marchan-Hernandez, E. Valencia, N. Rodriguez-Alvarez, I. Ramos-Perez, X. Bosch-Lluis, A. Camps, F. Eugenio, J. Marcello, "Sea-state determination using GNSS-R data," *IEEE Trans. Geosci. Remote Sens.*, vol. 7, no. 4, pp. 621-625, Apr. 2010.

[8] M.P. Clarizia, C.S. Ruf, P. Jales, C. Gommenginger, "Spaceborne GNSS-R minimum variance wind speed estimator", *IEEE Trans. Geosci. Remote Sens*,vol.52, no. 11, pp. 6829-6843, November 2014.

[9] M Martin-Neira, M.Caparrini, J. Font-Rossello, S. Lannelongue, C. S.Vallmitjana, "The PARIS concept: An experimental demonstration of sea surface altimetry using GPS reflected signals," *IEEE Trans. Geosci. Remote Sens.*, vol. 39, no. 1, pp. 142-150, Jan. 2001.

[10] M.Antoniou and M. Cherniakov, "GNSS-based bistatic SAR: A signal processing view," *EURASIP Journal on Advances in Signal Processing*, no.1, pp. 1-16, Mar. 2013.

[11] H.Ma, M. Antoniou, M. Cherniakov, "Passive GNSS-based SAR Resolution Improvement Using Joint Galileo E5 Signals," *IEEE Geosci. Remote Sens. Lett.*, vol. 12, no. 8, pp. 1640-1644, Aug. 2015.

[12] F. Liu, M. Antoniou, Z. Zeng, M. Cherniakov, "Coherent change detection using passive GNSS-based BSAR: experimental proof of concept," *IEEE Trans. Geosci. Remote Sens.*, vol. 51, no.8,pp. 4544-4555, Aug. 2013.

[13] Q. Zhang, M. Antoniou, W. Chang, M. Cherniakov, "Spatial de-correlation in GNSS-based SAR coherent change detection", *IEEE Trans. Geosci. Remote Sens.*, vol. 53, no. 1, pp. 219-228, January 2015.

[14] M. Conti, F. Berizzi, M. Martorella, E. DalleMese, D. Petri, A. Capria, "High range resolution multichannel DVB-T passive radar,"IEEE Aerosp. Electron. Syst. Mag., vol. 27, no. 10, pp. 37-42,Oct. 2012.

[15] F. Colone, D. W. O'Hagan, P. Lombardo, C. J. Baker, "A multistage processing algorithm for disturbance removal and target detection in passive bistatic radar," IEEE Trans. Aerosp. Electron. Syst.vol. 45, no. 2, pp. 698-722, Apr. 2009.

[16] X. Zhang, H. Li, B. Himed, "Multistatic detection for passive radar with direct path interference", IEEE Trans. Aeros. Elec. Sys., vol.53, no. 2, pp. 915-925, April 2017.

[17] F. Santi, M. Bucciarelli, D. Pastina, M. Antoniou, M. Cherniakov, "Spatial resolution improvement in GNSS-based SAR using multi-static acquisitions and feature extraction", *IEEE Trans. Geosci. Remote Sens.*, vol. 54, no. 10, pp. 6217-6231, October 2016.

[18] F. Pieralice, D. Pastina, F. Santi,M. Bucciarelli,H. Ma, M. Antoniou, M. Cherniakov, "GNSS-Based Passive Radar for Maritime Surveillance: Long Integration Time MTI Technique", in *IEEE Radar Conference*, Seattle, USA, May 2017.

[19] H. Ma, M. Antoniou, M. Cherniakov, D. Pastina, F. Santi, F. Pieralice,M. Bucciarelli, "Maritime target detection using GNSS-based radar: Experimental proof of concept", in *IEEE Radar Conference*, Seattle, USA, May 2017.

[20] G. Bournaka, A. Baruzzi, J. Heckenbach, H. Kuschel, "Experimental validation of beamforming techniques for localization of moving target in passive radar", in IEEE International Radar Conference 2015, pp. 1710-1713, May 2015.

[21] L. Lin, H. C. So, F. K. W. Chan, Y. T. Chan, K. C. Ho, "A new constrained weighted least squares algorithm for TDOA-based localization,"*Signal Processing*, vol. 93, no. 11, pp. 2872-2878, Nov. 2013.

[22] H. Schau and A. Robinson, "Passive source localization employing intersecting spherical surfaces from time-of-arrival differences," *IEEE Trans. Acoust., Speech, Signal Process.*, vol. 35, no.8,pp. 1223-1225, Aug. 1987.

[23] B. Amir, P. Stoica, and J. Li, "Exact and approximate solutions of source localization problems,"*IEEE Trans. Signal Process.*, vol. 56, no. 5, pp. 1770-1778, Apr. 2008.

[24] M. Malanowski and K. Kulpa, "Two methods for target localization in multistatic passive radar," *IEEE Trans. Aerosp. Electron. Syst.*, vol. 48, no. 1, pp. 572-580, Jan. 2012.

[25] M. Radmard, S. M. Karbasi, M. M. Nayebi, "Data fusion in MIMO DVB-T-based passive coherent location," *IEEE Trans. Aerosp. Electron. Syst.*, vol. 49, no.3, pp. 1725-1737, Jul. 2013.

[26] A. Noroozi and A. S. Mohammad, "Target localization from bistatic range measurements in multi-transmitter multi-receiver passive radar," *IEEE Signal Process. Lett.*, vol. 22, no. 12, pp. 2445-2449, Oct. 2015.

[27] M. Edrich, A. Schroeder and F. Meyer, "Design and performance evaluation of a mature FM/DAB/DVB-T multi-illuminator passive radar system," *IET Radar, Sonar & Navigation*, vol. 8, no. 2, pp. 114-122, Feb. 2014.

[28] H. Schau and A. Robinson, "Passive source localization employing intersecting spherical surfaces from time-of-arrival differences," *IEEE Trans. Acoust., Speech, Signal Process.*, vol. 35, no.8,pp. 1223-1225, Aug. 1987.

[29] G. Mellen, M. Pachter, J. Raquet, "Closed-form solution for determining emitter location using time difference of arrival measurements," *IEEE Trans. Aerosp. Electron. Syst.*, vol. 39, no.3, pp. 1056-1058, Jul. 2003.

[30] J. Smith and J. Abel, "The spherical interpolation method of source localization," *IEEE Journal of Oceanic Engineering*, vol. 12, no. 1, pp. 246—252, Jan.1987.

[31] SX3 GNSS Software Receiver Datasheet. [Online]. Available: http://www.ifen.com/fileadmin/user_upload/product_flyer/SX3.Datasheet_Letter.pdf.

[32] K. E. Olsen and K. Woodbridge, "Analysis of the Performance of a Multiband Passive Bistatic Radar Processing Scheme", on *Waveform Diversity and Design Conference (WDD), 2010 International*, Niagara Falls, ON, 2010, pp. 142-149.

[33] Q. Wu, Y. Zhang, M.G. Amin, B. Himed, "Space-Time Adaptive Processing and motion parameter estimation in multi-static passive radar using Bayesian learning", *IEEE Trans. Geosci. Remote Sens.*, vol. 54, no. 2, pp. 944-957, February 2016.